



# A DFT study of optoelectronic, elastic and thermo-electric properties of the double perovskites $\text{Rb}_2\text{SeX}_6$ ( $\text{X}=\text{Br}, \text{Cl}$ )

W. A. Yahya<sup>a,\*</sup>, A. A. Yahaya<sup>a,b</sup>, A. A. Adewale<sup>c</sup>, A. A. Sholagberu<sup>a</sup>, N. K. Olasunkanmi<sup>a</sup>

<sup>a</sup>Department of Physics and Materials Science, Kwara State University, Malete, Nigeria.

<sup>b</sup>Department of Physics, Kebbi State University of Science and Technology, Aliero, Nigeria.

<sup>c</sup>Department of Pure and Applied Physics, Ladoke Akintola University of Technology, Ogbomosho, Nigeria.

## Abstract

Thermo-electric (TE) material applications reduce reliance on traditional energy resources by converting heat to electric energy. We have studied, for the first time, the thermo-electric properties of  $\text{Rb}_2\text{SeX}_6$  ( $\text{X}=\text{Br}, \text{Cl}$ ). Using norm-conserving pseudo potentials in a plane wave basis set of Quantum Espresso code, the optoelectronic, elastic and thermo-electric properties of  $\text{Rb}_2\text{SeX}_6$  ( $\text{X}=\text{Br}, \text{Cl}$ ) have been investigated using density functional theory. Generalized Gradient Approximation of Perdew Burke Ernzerhof (GGA-PBE) and Generalized Gradient Approximation of Perdew Burke Ernzerhof adapted for Solid (GGA-PBESol) exchange correlation functionals were employed in all calculations. The band structure plots suggest that the studied double perovskites have indirect band gaps.  $\text{Rb}_2\text{SeBr}_6$  band gap values of 1.7574/ 1.569 eV (using GGA-PBE/PBESol) are remarkably similar to that of two effective inorganic/organic perovskites  $\text{FAPbI}_3$  and  $\text{MAPbI}_3$ . Maximum peaks generated from refractive index results indicate possible solar cell uses of the materials because they are in the visible and ultraviolet ranges. The results of other optical properties such as absorption coefficients, electron energy loss, conductivity, and reflectivity concludes that  $\text{Rb}_2\text{SeX}_6$  ( $\text{X}=\text{Br}, \text{Cl}$ ) have good values for electron generation, high potential for applications in the optoelectronic industry and are semiconductor in nature. The calculated shear anisotropy values of  $\text{Rb}_2\text{SeBr}_6/\text{Cl}_6$  are 3.09/1.71, suggesting that they are isotropic materials. With calculated Poisson's ratio of 0.32 and 0.26, the materials are predicted to be ductile in nature. The two materials are appropriate for thermo-electric applications since their thermal to electrical conductivity ratio are small (the order of  $10^{-5}$ ). The calculated minimum values of Seebeck coefficient values of  $0.198 \times 10^3 / 0.166 \times 10^3$  (m V/K) at 750 K, for  $\text{Rb}_2\text{SeBr}_6/\text{Cl}_6$  are positive, indicating that they have p-type conduction. Figure of merit values at all temperature range considered are greater than one ( $ZT > 1$ ) for both  $\text{Rb}_2\text{SeBr}_6$  and  $\text{Rb}_2\text{SeCl}_6$ , suggesting that they are good thermo-electric materials. The results of the calculations provide the basis for the industrial application of  $\text{Rb}_2\text{SeBr}_6/\text{Cl}_6$  as solar cells.

DOI:10.46481/jnsps.2023.1418

**Keywords:** Double perovskite, opto-electronic properties, elastic properties, Seebeck coefficients, Figure of merit, DFT.

## Article History :

Received: 24 February 2023

Received in revised form: 21 April 2022

Accepted for publication: 28 April 2023

Published: 29 April 2023

© 2023 The Author(s). Published by the Nigerian Society of Physical Sciences under the terms of the Creative Commons Attribution 4.0 International license (<https://creativecommons.org/licenses/by/4.0>). Further distribution of this work must maintain attribution to the author(s) and the published article's title, journal citation, and DOI.

Communicated by: Babatunde James Falaye (PhD)

\*Corresponding author tel. no: +2348036289110  
Email address: wasiu.yahya@gmail.com &  
wasiu.yahaya@kwasu.edu.ng (W. A. Yahya)

## 1. Introduction

Economic sustainability, human growth and developments can be achieved with a reliable, efficient, and consistent supply of energy. In some places, access to energy can be viewed as a golden thread for the growth of a human being and its economy

[1]. Due to the increased need for energy, researchers are looking for ways to avoid using fossil fuels, which are harmful to our ecosystem. Sunlight, together with tidal energy, wind energy, hydrothermal energy, and other renewable energy sources, are abundant, infinite, and nontoxic [2, 3]. Many efforts have been made by researchers to develop low-cost, environmental friendly systems that can harness the solar energy spectrum, as an alternative source of electricity [4, 5]. Solar energy, being the most important renewable energy source, has played a key role and thus demonstrated varying performance depending on the material used in photovoltaic (PV) modules [6]. Currently, the search for an appropriate material is a primary motivation for researchers, and extensive research is being conducted to identify their potential applications in opto-electronics [2, 6–9].

Perovskite structure materials are one of the emerging technologies for solar power with cheap manufacturing costs and materials that are altering renewable energy technology. due to their industrial and technological wide applications such as optoelectronic materials, half metallic materials, thermo-electric materials, spintronic materials, ferromagnetic materials, semiconductors, magneto optic materials, and so on [10–12]. Perovskite studies have received a lot of attention, both theoretically and experimentally [10, 12]. Perovskite has a wide range of applications due to its unique tuneable structure, impurity addition, and material atom substitutions (vacancy). Several investigations on double perovskite solar cells have showed good environmental stability and intriguing optoelectronic features [7, 9, 13, 14]. Perovskite is a fantastic material for many technologies, but it has narrow electrical conductivity, toxicity, and structural instabilities which limits its use in technical application [1, 15–17].

In 2022, [9] investigated the crystal structure of inorganic halide double perovskite  $A_2BX_6$ . They used the octahedral factor and the radius ratio to forecast the development and deformation of the structure, where  $A = Cs$  and  $Rb$ ,  $B = Ge$ ,  $Zr$ ,  $Sn$ ,  $Hf$ ,  $Se$ ,  $Te$ , and  $Pd$ , and  $X = I$ ,  $Cl$ ,  $Br$ , yielding 42 compounds. The energy band gaps of 14 different types of crystalline PV crystals ranged from 1.33 eV to 2.40 eV. Some materials, such as  $Cs_2ZrI_6$ ,  $Cs_2HfI_6$ ,  $Cs_2SeI_6$ ,  $Cs_2TeI_6$ ,  $Rb_2HfBr_6$ ,  $Rb_2GeCl_6$ ,  $Cs_2SeBr_6$ , and  $Rb_2HfBr_6$ , exhibit conduction band minimum edges greater than 4.6 eV and valence band maximum edges less than - 5.4 eV. The light absorption curves of  $Cs_2SeI_6$ ,  $Cs_2SeBr_6$ ,  $Rb_2SeBr_6$ , and  $Rb_2SeCl_6$  span a large range in the visible light spectrum. The molecules containing Cs and Rb are nearly identical, and the Cs-containing perovskite crystals are more stable. The band gap size and light absorption qualities of  $Rb_2SeI_6$ ,  $Rb_2SeBr_6$ , and other compounds make them suitable alternatives for light absorption materials. The two materials considered in the current study were included in their research. However, the thermo-electric properties were not investigated. This study aims to investigate the thermo-electric properties of  $Rb_2SeBr_6/Cl_6$ .

[18] used a theoretical method to investigate the structural, mechanical, and optoelectronic properties of lead-free double

perovskites  $A_2SeX_6$  ( $A=Rb, K; X=Cl, Br, I$ ). Their findings show that these  $A_2SeX_6$  ( $A=Rb, K; X=Cl, Br, I$ ) double perovskites are ductile as well as structurally and mechanically stable. Their electronic structure calculation shows that these double perovskite materials are indirect band gap semiconductors. As suggested by [18],  $A_2SeCl_6$  and  $A_2SeBr_6$  can be used to make a variety of optoelectronic devices such as photodetectors, solar cells, light-emitting diodes, and so on.

The optoelectronic, optical, elastic and thermo-electric properties of the double perovskites  $Rb_2SeX_6$  ( $X=Br, Cl$ ) have been investigated in this work utilizing density functional theory (DFT) first principle approaches. GGA-PBE and GGA-PBESol exchange-correlation functionals were utilized to evaluate atomic interactions. We have, for the first time, investigated the thermo-electric properties of  $Rb_2SeBr_6/Cl_6$ . The calculations have been carried out using a norm-conserving pseudo potential as implemented in the plane wave Quantum Espresso algorithm. This article is organized as follows: Section 2 describes the computational details, followed by results presentation and discussions in Section 3. Section 4 contains the conclusion.

## 2. Computational Details

In this study, norm-conserving pseudo potentials were used in the calculation of optoelectronic, elastic and thermo-electric properties of  $Rb_2SeX_6$  ( $X=Br, Cl$ ) using plane wave methods as implemented in the Quantum-Espresso code [19, 20] using GGA-PBE and GGA-PBESol exchange correlation functionals [21]. The energy cut-off convergence was set at 120 Ry and Brillouin zone integration sampling with k-point mesh  $6 \times 6 \times 6$  Monkhorst-Pack [22] was employed for the electronic and elastic properties calculations. The force and energy convergence thresholds were  $10^{-5}$  eV  $\text{\AA}^{-1}$  and  $10^{-5}$  eV per atom, respectively.

Thermo-electric properties such as electrical conductivity ( $\sigma$ ), electronic thermal conductivity ( $\kappa_e$ ), Seebeck coefficient (S), power factor (PF), and figure of merit (ZT) were investigated in this study using GGA-PBE and GGA-PBESol via the generalized semi-classical BoltzTraP2 package [37], which works within the framework of density functional theory (DFT) as implemented in Quantum ESPRESSO code, under the constant relaxation time approximation ( $\tau = 10^{-14}$ s). Calculated values of S and  $\kappa_e$  depend linearly on  $\tau$  within this constant  $\tau$  approximation, and ZT depends strongly on these TE parameters.

The electronic, optical, elastic and thermo-electric properties of the  $Rb_2SeX_6$  ( $X=Br, Cl$ ) double perovskite materials were investigated using both GGA-PBE and GGA-PBESol [21] exchange correlation functionals. To further investigate the origin of the electronic band structure, the total density of states (TDOS) and partial density of states (PDOS) of  $Rb_2SeX_6$  ( $X=Br, Cl$ ) double perovskite material were calculated. For the thermo-electric properties, k-points of  $18 \times 18 \times 18$

was employed. The locations of the atoms were completely optimized for optical characteristics and density of state, Broyden-Fletcher-Goldfarb-Shanno quasi-Newton algorithm (BFGS) was utilized for complete structural relaxation [23, 24].

### 2.1. Calculation of Optical Properties

One of the crucial criteria for the selection of high-performance solar cells is their optical properties, which play a significant role and can be correlated with electronic structures for necessary explanations [25]. When an appropriate ray of light in the form of a photon is impinging on a material, it will result in some properties known as optical properties [7]. It is critical because it demonstrates how efficiently PV materials absorb energy (photons) when they fall on them [26–28]. Strong optical absorbance and large dielectric constant are highly required. The linear response approach can be used to determine the dielectric function expression [25–27]:

$$\varepsilon(\omega) = \varepsilon_1(\omega) + i\varepsilon_2(\omega), \quad (1)$$

where  $\varepsilon_1(\omega)$  and  $\varepsilon_2(\omega)$  represent the real and imaginary dielectric tensor components, respectively. The real part of the dielectric tensor component shows how much light is polarized by incident light at the plasmonic resonance frequency and how this varies with photon energy, whereas the imaginary part of the dielectric tensor shows how much light is absorbed by the material [26, 27, 29]. Furthermore, optical features of materials enable relevant instruments to examine the energy band structure, lattice vibrations, impurity levels, and exciton, among other things [26, 27]. The real and imaginary parts of dielectric tensors are given as follows using Kramers-Kronig [30] relations:

$$\varepsilon_1(\omega) = \frac{2}{\pi} \rho \int_0^{\infty} \frac{\omega'^2 \varepsilon_2 \omega}{\omega'^2 - \omega^2}, \quad (2)$$

$$\varepsilon_2(\omega) = \frac{-2}{\pi} \rho \int_0^{\infty} \frac{\omega'^2 \varepsilon_2 \omega}{\omega'^2 - \omega^2}. \quad (3)$$

The reflectivity ( $R(\omega)$ ), refractive index ( $n(\omega)$ ), optical conductivity ( $Re(\sigma)$ ), energy loss spectrum ( $L(\omega)$ ), extinction coefficient ( $K(\omega)$ ), and absorption coefficient ( $I(\omega)$ ) as photon energy functions within the range of 0 - 30 eV are determined for  $Rb_2SeX_6$  ( $X=Br, Cl$ ). GGA-PBE and GGA-PBEsol exchange correlation functionals were used in optical properties calculation in this work. The other optical properties, such as optical conductivity ( $Re(\sigma)$ ), refractive index ( $n(\omega)$ ), extinction coefficient ( $K(\omega)$ ), electron energy loss spectrum ( $L(\omega)$ ), reflectivity ( $R(\omega)$ ) and absorption coefficient ( $I(\omega)$ ) have been computed using:

$$Re(\sigma) = \frac{\omega}{4\pi} \varepsilon_2(\omega), \quad (4)$$

$$n(\omega) = \sqrt{\frac{|\varepsilon(\omega)| + \varepsilon_1(\omega)}{2}}, \quad (5)$$

$$K(\omega) = \sqrt{\frac{|\varepsilon(\omega)| - \varepsilon_1(\omega)}{2}}, \quad (6)$$

$$L(\omega) = \frac{\varepsilon_2}{\varepsilon_1^2 + \varepsilon_2^2}, \quad (7)$$

$$R(\omega) = \frac{(n-1)^2 + k^2}{(n+1)^2 + k^2}, \quad (8)$$

$$I(\omega) = \sqrt{2} \omega \left( \frac{\varepsilon_1(\omega)^2 + \varepsilon_2(\omega)^2 - \varepsilon_1(\omega)}{2} \right)^{\frac{1}{2}}. \quad (9)$$

### 2.2. Calculation of Mechanical Properties

During materials manufacturing process, it's necessary to provide mechanical and elastic properties of the material so that the detailed knowledge of the material will be known [7, 31]. During the process of fabricating a material, forces may be applied to it, this makes it vital to understand the nature of solid forces and its atomic dynamical behaviour [7, 31] before applying forces to that material. The elastic constant  $C_{ij}$  of a material directly proves its strength and stability. Max Born and Kun Huang developed the Born-Huang theory [32], which provides a broad explanation of a material's mechanical stability and was later examined by L. Max [32]. The theorem is Born-Huang elastic criteria. The stability criteria for cubic crystal structure are given as follows [32]:

$$C_{11} - C_{12} > 0, \quad (10)$$

$$C_{11} - 2C_{12} > 0, \quad (11)$$

$$C_{44} > 0, \quad (12)$$

$$C_{11} < B < C_{44}, \quad (13)$$

where  $B$  is the bulk modulus. If a material's  $C_{12}$  value is low, it implies that the material will compress more easily in the  $C_{12}$  direction than in any other direction [7, 33]. Voigt, Reuss [34], and Hills [35] established a link between the elastic constant and several isotropic properties such as bulk modulus, shear modulus, and young modulus. Chung and Buessem combined this relationship into the Voigt-Reuss-Hill Approximation (VHR) [36]. The bulk modulus of a material is a measure of its strength which may be computed using the formula:

$$B = \frac{C_{11} + 2C_{12}}{3}. \quad (14)$$

The shear modulus of a material is a measurement of its capacity to resist transverse deformations in relation to its hardness. It defines a material's plastic deformation to resistance; a greater value of shear modulus describes the material's ductility. High shear modulus value implies that the material will be very difficult to change shape or form. The values of shear anisotropy ( $A$ ), internal strain factor ( $\xi$ ), Young's modulus ( $Y$ ), Poisson's ratio ( $\nu$ ), Pugh's ratio ( $R_p$ ) and Frantsevich's ratio ( $R_f$ ) were, respectively, calculated using the following:

$$A = \frac{2C_{44}}{C_{11} - C_{12}}, \quad (15)$$

$$\xi = \frac{(C_{11} + 8C_{12})}{7(C_{11} + 2C_{12})} \quad (16)$$

$$Y = \frac{9BG}{3B + G}. \quad (17)$$

$$v = \frac{3B - 2G}{6B + 2G}. \quad (18)$$

$$R_p = \frac{B}{G}, \quad (19)$$

$$R_f = \frac{G}{B}, \quad (20)$$

### 2.3. Calculation of Thermo-electric Properties

The Boltztrap2 code [37] was used to calculate the thermo-electric properties. The code calculates the Seebeck coefficient ( $S$ ), electrical conductivity ( $\sigma$ ), and thermal conductivity ( $\kappa_e$ ) at various temperature ( $T$ ) values. The power factor (PF) is then obtained by multiplying electrical conductivity with the square of Seebeck coefficient [38, 39]:

$$PF = S^2 \sigma \quad (21)$$

The figure of merit ( $ZT$ ) is computed using the following formulae [71]:

$$ZT = \frac{\sigma S^2}{\kappa_e} T. \quad (22)$$

## 3. Results and Discussion

### 3.1. Electronic Properties

The band structure of a material reveals information about its conductivity nature, which also connects optical and electronic properties with the crystal structure [40]. This section presents the results of the band structure and density of states calculations of  $\text{Rb}_2\text{SeX}_6$  ( $X=\text{Br}, \text{Cl}$ ). Band structures and density of states are very important parameters when building an optoelectronic device.

#### 3.1.1. Band structure

Band structure plots for  $\text{Rb}_2\text{SeBr}_6$  and  $\text{Rb}_2\text{SeCl}_6$  was shown in Figures 1 and 2, respectively. It can be observed from the Figures that the valence band maximum (VBM) and conduction band minimum (CBM) do not lie at the same symmetry point. The Figures also show that  $\text{Rb}_2\text{SeX}_6$  ( $X=\text{Br}, \text{Cl}$ ) have indirect band gaps.  $\text{Rb}_2\text{SeBr}_6$  has CBM = - 4.6317 eV and VBM = - 3.0627 eV, whereas  $\text{Rb}_2\text{SeCl}_6$  has CBM = - 5.1639 eV and VBM = -2.7141 eV. Given the energy band values of indium tin oxide (ITO), Silver (Ag) and poly(3,4-ethylenedioxythiophene) polystyrene sulfonate (PEDOT:PSS), the minimum edge of the conduction band must be more than 4.6 eV, and the highest value of the valence band must be less than 5.4 eV [41, 42]. The aforesaid conditions are met by the double perovskite materials in this work as shown in Table 1.

Table 1 displays the calculated band gaps for the double perovskite materials. The band gap results show that there is an increase in the band gap value when the cations is changed from Br to Cl halogen anions;  $\text{Rb}_2\text{SeCl}_6$  has higher band gap (2.6115

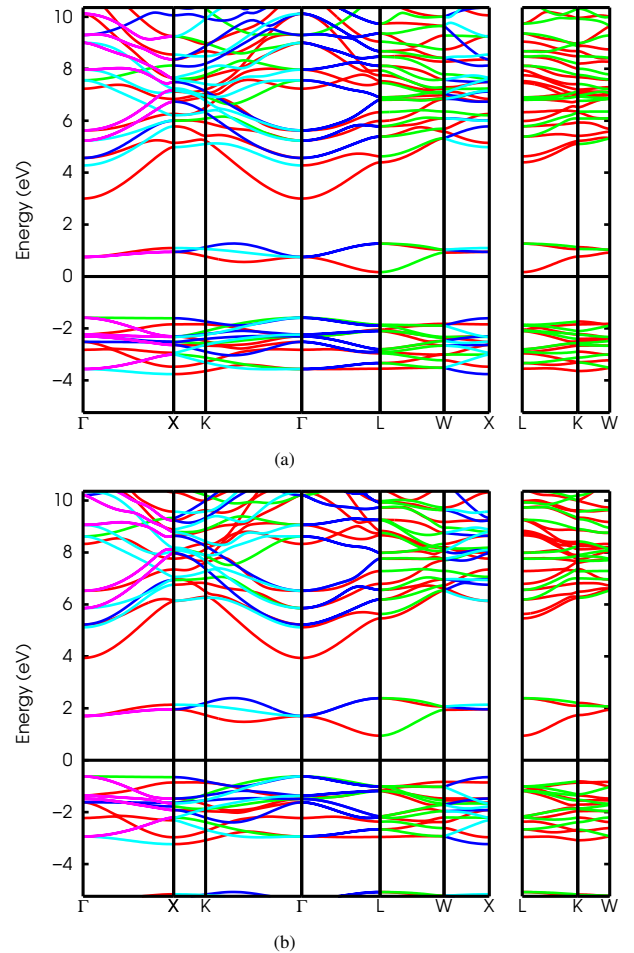


Figure 1: Band structure plots of  $\text{Rb}_2\text{SeBr}_6$  using (a) GGA-PBE and (b) GGA-PBESol.

Table 1: Electronic band gap of studied double perovskite using GGA-PBE and GGA-PBESol.

Material	GGA-PBE (eV)	GGA-PBESol (eV)	Other Calculations (eV)
$\text{Rb}_2\text{SeBr}_6$	1.7574	1.569	1.775 [9], 1.93 [9], 1.60 [18], 2.37 [18]
$\text{Rb}_2\text{SeCl}_6$	2.6115	2.4498	2.819 [9], 2.912 [9], 2.48 [18], 3.20 [18]

eV and 2.4498 eV) than  $\text{Rb}_2\text{SeBr}_6$  (1.7574 and 1.569). The computed band gap results are comparable to those reported by [9] and [18] for all the double perovskite materials. From the result,  $\text{Rb}_2\text{SeBr}_6$  has a band gap value that is very close to the band gap values of two efficient inorganic/organic perovskite forms ( $\text{NH}_2\text{CH}=\text{NH}_2\text{PbI}_3$ )  $\text{FAPbI}_3$  and ( $\text{CH}_3\text{NH}_3\text{PbI}_3$ )  $\text{MAPbI}_3$ . The calculated band gap of  $\text{Rb}_2\text{SeBr}_6$  using PBESol is also quite near to the Shockley-Queisser theory of optimum band gap energy ( $E_g$ ) for high-efficiency solar cells, which is in the 1.3 eV to 1.4 eV range [29, 43, 44].

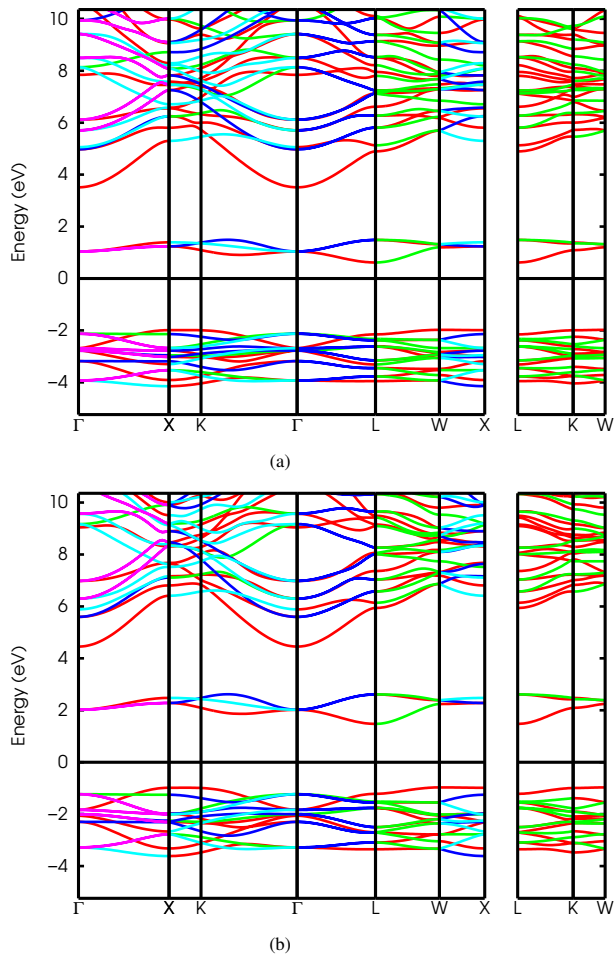


Figure 2: Band structure plots of  $\text{Rb}_2\text{SeCl}_6$  using (a) GGA-PBE and (b) GGA-PBESol.

### 3.1.2. Density of State (DOS)

Figures 3 and 4 show plots of the computed TDOS using GGA-PBE and GGA-PBESol exchange correlational functionals. The Figures clearly show that conduction bands and valence bands do not cross the Fermi energy level. The result also confirms that the two double perovskite materials are semiconductor in nature.

The PDOS (Projected Density of State) was studied to investigate atomic orbitals contribution of each atom, Figures 5 and 6 show the PDOS plots of the studied double perovskites  $\text{Rb}_2\text{SeX}_6$  ( $X=\text{Br}, \text{Cl}$ ) using both GGA-PBE and GGA-PBESol. From the plots of  $\text{Rb}_2\text{SeBr}_6$ , Se-3p orbital is the most dominant in the VBM followed by Br-2p orbital, while in CBM, Br-2p is the most dominant then followed by Se-2s orbitals, Se and Br have contributed in obtaining a good value of band gap in  $\text{Rb}_2\text{SeBr}_6$  double perovskite using both GGA-PBE and GGA-PBESol. From the plots  $\text{Rb}_2\text{SeCl}_6$ , Se-3p orbital is the most dominant in the VBM followed by Cl-2p orbital, and in CBM Cl-2p is the most dominant, followed by Se-2s and then Rb-3s orbitals; this contributes in obtaining value of band gap of  $\text{Rb}_2\text{SeCl}_6$  double perovskite materials. Other atoms in the stud-

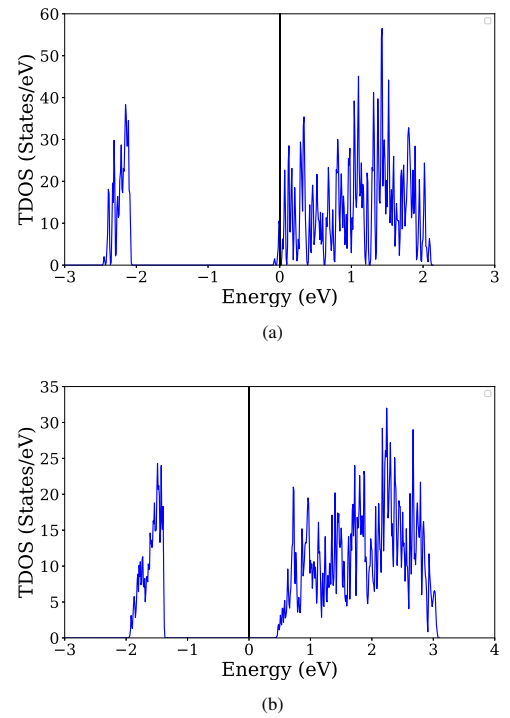


Figure 3: Total density of states (TDOS) of (a) GGA-PBE  $\text{Rb}_2\text{SeBr}_6$  and (b) GGA-PBESol  $\text{Rb}_2\text{SeBr}_6$ .

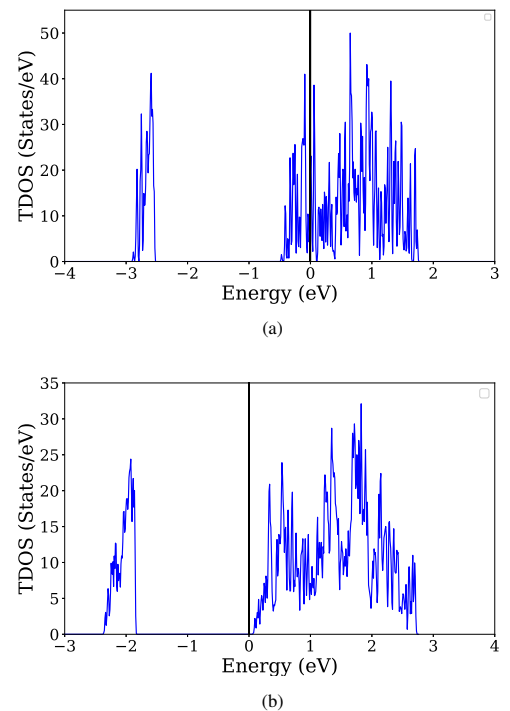


Figure 4: Total density of states (TDOS) of  $\text{Rb}_2\text{SeCl}_6$  using (a) GGA-PBE and (b) GGA-PBESol.

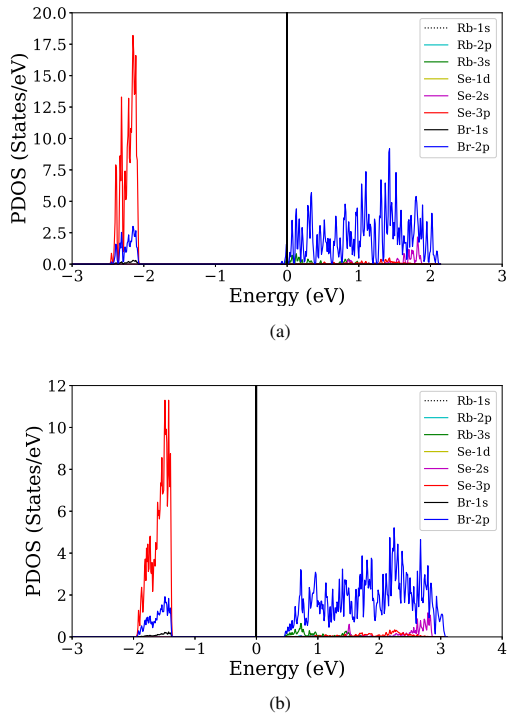


Figure 5: Partial density of states (PDOS) of  $\text{Rb}_2\text{SeBr}_6$  using (a) GGA-PBE and (b) GGA-PBESol

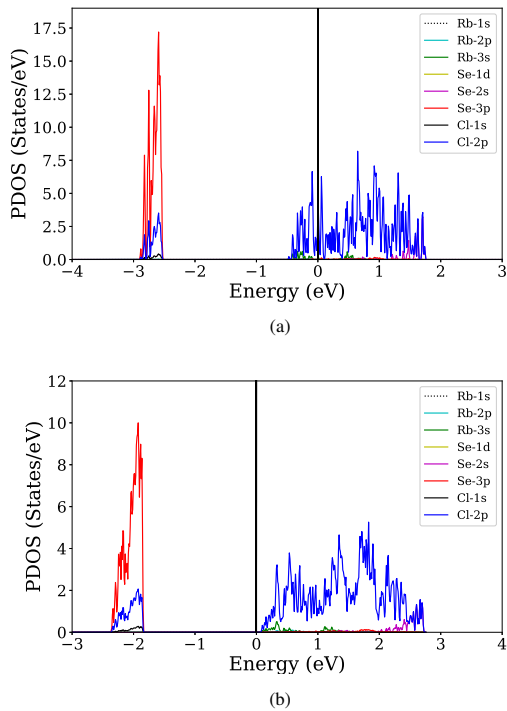


Figure 6: Partial density of states (PDOS) of  $\text{Rb}_2\text{SeCl}_6$  using (a) GGA-PBE and (b) GGA-PBESol

ied double perovskite materials have little or no contribution to both CBM and VBM of the studied double perovskite materials.

### 3.2. Optical properties

The calculated dielectric function of the investigated double perovskite is based on inter-band transitions, which correspond to the electronic band gaps. Figure 7 shows the plots of the real part of the dielectric functions  $\epsilon_1(\omega)$ . From the figure,  $\epsilon_1(\omega)$  depends strongly on band gap and it has a static value which is part of the electronic static dielectric constant.  $\text{Rb}_2\text{SeBr}_6$  has static values of 5.7 and 6.3 for GGA-PBE and GGA-PBESol, respectively, and  $\text{Rb}_2\text{SeCl}_6$  has static values of 4.5 and 4.9 for GGA-PBE and GGA-PBESol, respectively.  $\text{Rb}_2\text{SeBr}_6$  has higher polarizability than  $\text{Rb}_2\text{SeCl}_6$ . The values of real dielectric function obtained in this result are comparable with these reported in [9].

The spectrum of the imaginary component of the dielectric function describes the response generated by incident electromagnetic radiation to the material, which also causes a shift in inter band that is related with the absorption of radiation in valance band occupied states [45]. The imaginary part of the dielectric constant is used to calculate the optical band gap, the optical gap is related to the threshold peak of the imaginary part of the dielectric function, which is a threshold energy value for absorbing a photon and creating an electron-hole pair [46]. The excitonic peaks of all substances are in the band gap energy range. When the visible range of energy matches the excitonic range of energy, the material has a low reflectivity and a high absorption coefficient [7, 47]. Figures 7 - 14 show the plot of optical properties results in this work. From the plots,  $\text{Rb}_2\text{SeBr}_6$  (9.2 at 4 eV and 8.6 at 4 eV) has higher peak than  $\text{Rb}_2\text{SeCl}_6$  (6.7 at 4 eV and 6.3 at 4 eV).

At zero energy, the values of refractive index is called static refractive index [48]. The calculated static refractive index values for  $\text{Rb}_2\text{SeBr}_6$  are 2.40 and 2.50 using GGA-PBE and GGA-PBESol, respectively, while for  $\text{Rb}_2\text{SeCl}_6$ , they are 2.13 and 2.25 using GGA-PBE and GGA-PBESol, respectively; this is shown in Figure 9. Maximum refractive index of around 29 - 32 were obtained for the studied double perovskite materials within the range of photon energies of 3 - 3.5 eV, and the minimum was obtained at photon energies of around 22 eV. Maximum peaks generated from refractive index results indicate possible solar cell uses of the materials because they are in the visible and ultraviolet ranges.

The amplitude of incident waves and reflected waves is used to calculate the reflection coefficient  $R(\omega)$  [18]. The reflectivity of a semiconductor material estimates the quantity of incident light that falls on it [49]. The lower the reflectivity of a material, the greater is its absorption of visible and UV light [49].  $\text{Rb}_2\text{SeBr}_6$  and  $\text{Rb}_2\text{SeCl}_6$  show reflectivity values in the range of 0.24-0.37 at photon energies of around 3.5-4.0 eV for both GGA-PBE and GGA-PBESol, respectively, as shown in Figure 10, but there is a reduction in reflection at

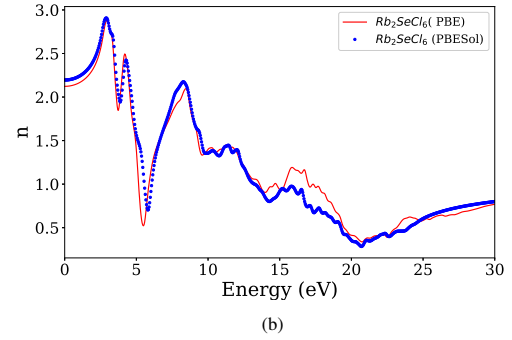
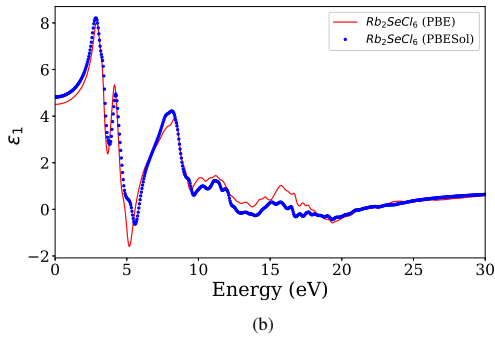
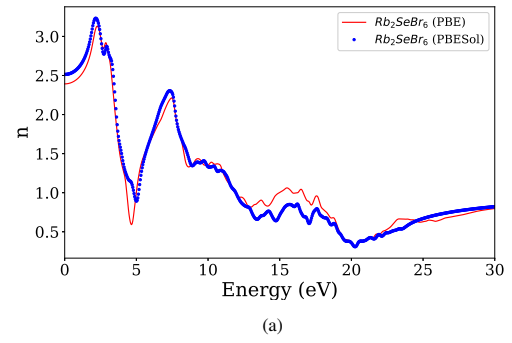
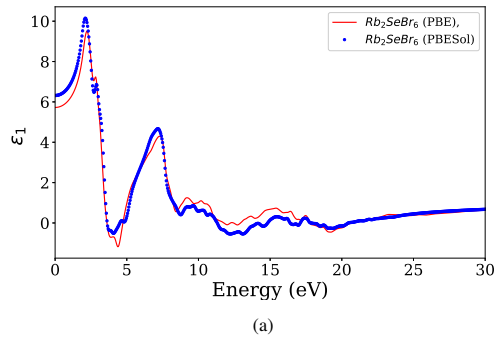


Figure 7: Real dielectric function plots of (a)  $Rb_2SeBr_6$  and (b)  $Rb_2SeCl_6$  using GGA-PBE and GGA-PBESol.

Figure 9: Refractive index plots of (a)  $Rb_2SeBr_6$  and (b)  $Rb_2SeCl_6$  using GGA-PBE and GGA-PBESol.

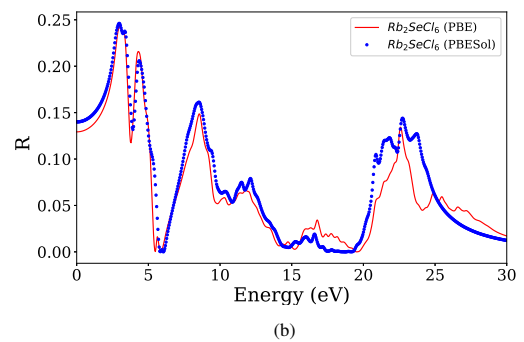
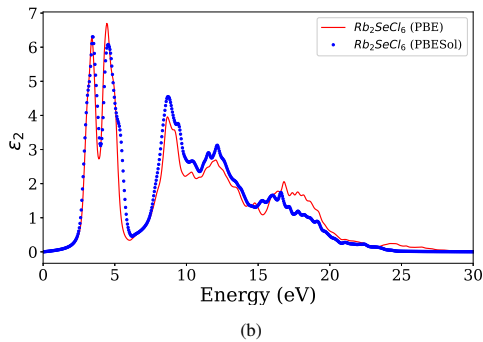
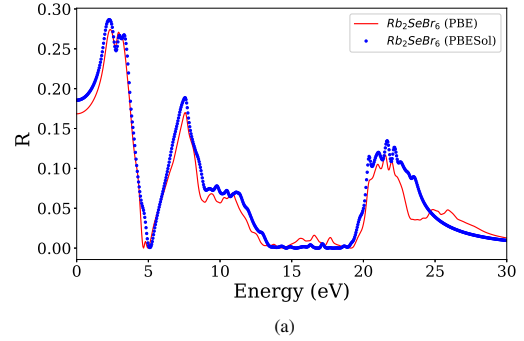
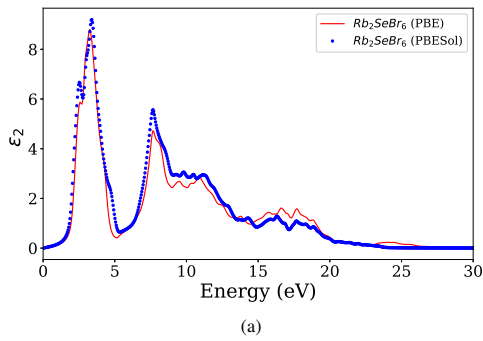


Figure 8: Imaginary dielectric function plots of (a)  $Rb_2SeBr_6$  and (b)  $Rb_2SeCl_6$  using GGA-PBE and GGA-PBESol.

Figure 10: Reflectivity plots of (a)  $Rb_2SeBr_6$  and (b)  $Rb_2SeCl_6$  using GGA-PBE and GGA-PBESol.

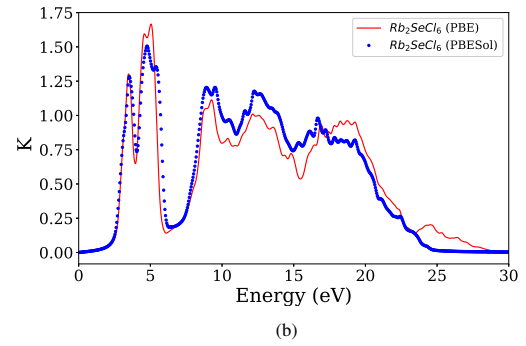
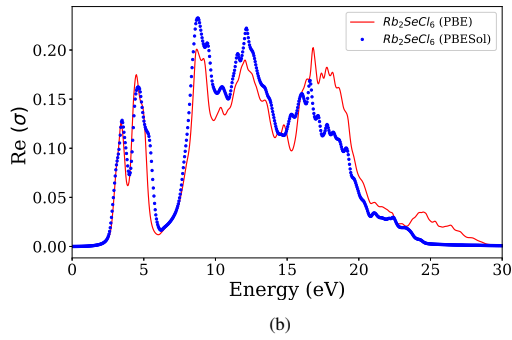
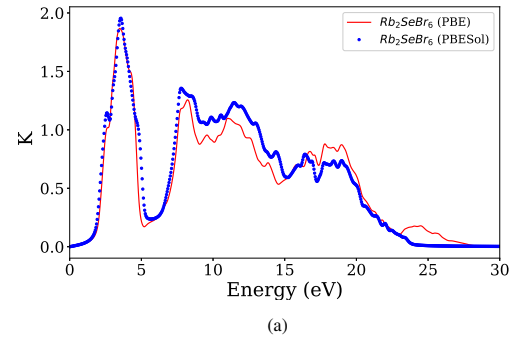
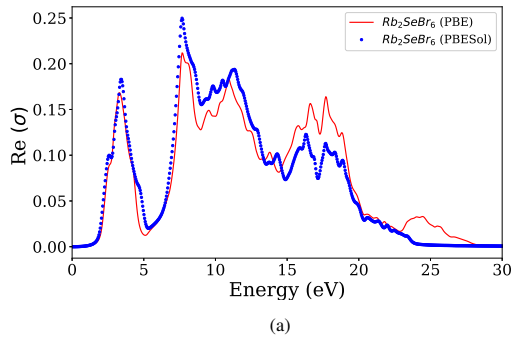


Figure 11: Optical conductivity plots of (a)  $Rb_2SeBr_6$  and (b)  $Rb_2SeCl_6$  using GGA-PBE and GGA-PBESol.

Figure 13: Extinction coefficient plots of (a)  $Rb_2SeBr_6$  and (b)  $Rb_2SeCl_6$  using GGA-PBE and GGA-PBESol.

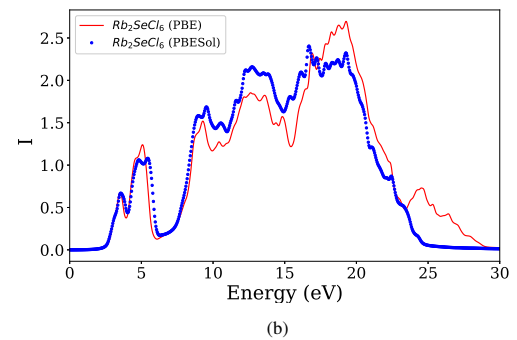
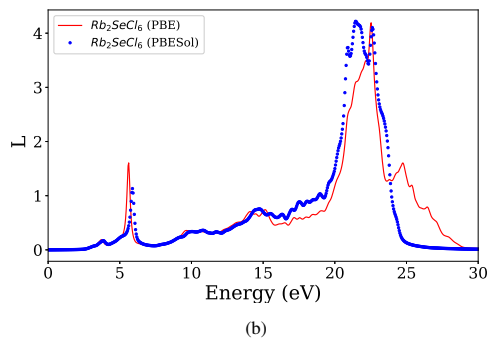
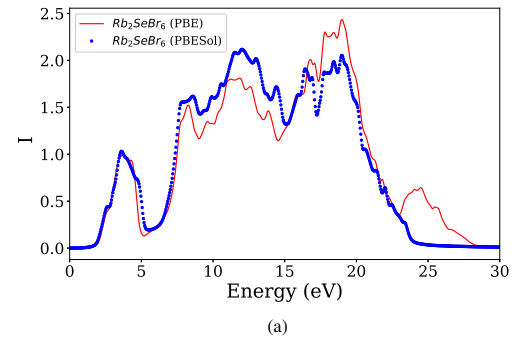
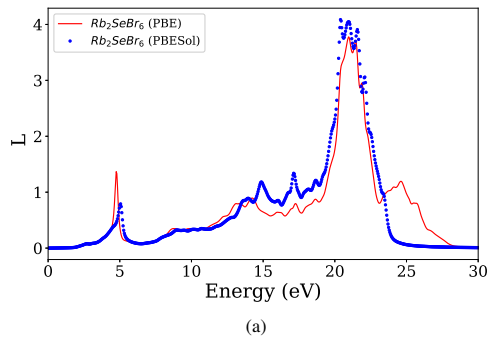


Figure 12: Electron energy loss plots of (a)  $Rb_2SeBr_6$  and (b)  $Rb_2SeCl_6$  using GGA-PBE and GGA-PBESol.

Figure 14: Absorption coefficient plots of (a)  $Rb_2SeBr_6$  and (b)  $Rb_2SeCl_6$  using GGA-PBE and GGA-PBESol.

around 5.5-6.0 eV for the two materials. It is possible to conclude that both  $\text{Rb}_2\text{SeBr}_6$  and  $\text{Rb}_2\text{SeCl}_6$  can be employed in optoelectronic applications.

The optical conductivity ( $\sigma$ ) reveals free electron creation as a result of incident energy absorption [8, 50]. Figure 11 depicts the optical conductivity of the studied double perovskite materials, which is proportional to the imaginary component of dielectric function [48]. According to the figure, conductivity starts at a static value of 0, it then increases to a higher value within the range of 0.23-0.25 at around 8.0-10.0 eV for both  $\text{Rb}_2\text{SeBr}_6$  and  $\text{Rb}_2\text{SeCl}_6$ , and then gradually decreases until it reaches the lowest values at around 24-25 eV.

An electron energy loss spectrum (EELS) can be used to characterize nanostructures and microstructures. Inter-band, intra-band, and plasmon interactions are defined by the electron energy-loss function. EELS is the energy lost by a fast-moving electron of electromagnetic light when it passes through a medium [51]. The plots of the studied double perovskites shows that the highest peak began at roughly 20 eV in the UV zone for the two double perovskite materials, which is attributable to electron energy loss induced by incident light inelastic electron scattering as shown in Figure 12.

The extinction coefficient reveals a material's ability to hold incident light, which is one of the features of optoelectronic materials [52]. It also expresses material behavior in terms of electromagnetic radiation attenuation at a specific wavelength [51]. Figure 13 shows the plots of extinction coefficients, which indicates higher values of around 1.5-1.8 at photon energy values of around 4-5 eV for both  $\text{Rb}_2\text{SeBr}_6$  and  $\text{Rb}_2\text{SeCl}_6$ . The extinction coefficient  $K(\omega)$  decrease after its peaks value, indicating clear declination in  $K(\omega)$  within higher energy range of UV region. Due to electromagnetic radiation in elastic scattering such as photoelectric effect, compton effect, etc., the region clearly reveals difference in  $K(\omega)$  [53, 54].

Figure 14 depicts the optical absorption plots of the investigated double perovskite materials; the plots illustrate the percentage attenuation of light intensity that propagates per unit distance in a material. According to the plots, both  $\text{Rb}_2\text{SeBr}_6$  and  $\text{Rb}_2\text{SeCl}_6$  have high absorption value of roughly 2.1-2.35 within the region of 10-22 eV photon energy. Due to the phonon energy within the forbidden band, they also reveal that the materials are transparent from partially ultra-violet to some visible light area (0-4 eV).  $\text{Rb}_2\text{SeBr}_6$  has higher value than  $\text{Rb}_2\text{SeCl}_6$ . Both  $\text{Rb}_2\text{SeBr}_6$  and  $\text{Rb}_2\text{SeCl}_6$  have high absorption coefficients and wider absorption range, making them potential materials for use in the optoelectronic industry.

### 3.3. Elastic properties

The result of computed values of bulk modulus, shear modulus, Young modulus, and Poisson's ratio for  $\text{Rb}_2\text{SeBr}_6$  and  $\text{Rb}_2\text{SeCl}_6$  are shown in Table 2. Young's modulus ( $Y$ ) deals with a material's stiffness. It displays the overall strength of a material [7]. From Table 2, Young modulus values are higher than the bulk modulus values, this indicates that the material

will be very hard to break [55]. Higher B values can indicate good crystal formation. If shear anisotropy ( $A$ ) of a material equals one, the material is said to be isotropic [55]. From Table 2, the anisotropy values of the two materials are greater than one. The estimated shear anisotropy values of  $\text{Rb}_2\text{SeBr}_6$  and  $\text{Rb}_2\text{SeCl}_6$  using both GGA-PBE and GGA-PBESol indicate that they are isotropic double perovskite materials.

The Poisson's ratio is a supportive parameter for determining crucial solid-material qualities like brittleness or ductility, shear stability, and the nature of interatomic force [7, 54]. A material with a Poisson's ratio less than 0.26 is said to be brittle, whereas a material with a Poisson's ratio more than 0.26 is a ductile material. The result of  $\text{Rb}_2\text{SeCl}_6$  is comparable with result reported by [18]. Using GGA-PBE, the Poisson ratio values of  $\text{Rb}_2\text{SeBr}_6$  and  $\text{Rb}_2\text{SeBr}_6$  are greater than 0.26, suggesting that they are ductile in nature. This is consistent with the results reported by [18]. The use of GGA-PBESol, however, suggest that the two materials are brittle in nature, since the Poisson ratio values are  $\leq 0.26$ . This is also in consonant with the results obtained in [9].

Cauchy pressure ( $C_{12} - C_{44}$ ), Pugh's ratio ( $R_p$ ) and Frantsevich's ratio ( $G/B$ ) can also be used to forecast the ductility or brittleness of a material [54]. Negative values of Cauchy pressure indicates brittleness of a material, while a positive value indicates materials ductility. The computed Cauchy pressure results for both  $\text{Rb}_2\text{SeBr}_6$  and  $\text{Rb}_2\text{SeCl}_6$  indicate that both are ductile in nature, except the calculation of the Cauchy pressure of  $\text{Rb}_2\text{SeCl}_6$  using GGA-PBESol, which suggests that  $\text{Rb}_2\text{SeCl}_6$  is brittle. Pugh's ratio ( $R_p$ ) is the ratio of bulk modulus to shear modulus ratio. A material is said to be brittle if the Pugh's ratio is less than 1.75; otherwise, it is ductile [54, 55]. The computed values of Pugh's ratio ( $R_p$ ) for  $\text{Rb}_2\text{SeBr}_6$  and  $\text{Rb}_2\text{SeBr}_6$  are greater than 1.75. The inverse of Pugh's ratio is termed as Frantsevich's ratio ( $R_f$ ). Frantsevich's ratio ( $R_f$ ) of a material must be greater than 0.571 for a material to be ductile; otherwise, the material is brittle [54]. The calculated Frantsevich's ratios ( $R_f$ ) for  $\text{Rb}_2\text{SeBr}_6$  and  $\text{Rb}_2\text{SeCl}_6$  indicate that they are ductile, because the calculated values are larger than 0.571. Overall, one can conclude that the two materials are ductile in nature.

Debye temperature is a solid characteristic that is related to thermodynamic properties of materials such as entropy, thermal expansion, and vibrational internal energy [56]. Debye temperature is the fundamental factor that provides some insight into thermodynamic behaviors from the standpoint of mechanical quantities that may be acquired from the average sound velocity [57]. Higher Debye temperatures indicate increase in thermal conductivity and stronger covalent bonds or bond strength in the materials [56, 57].  $\text{Rb}_2\text{SeCl}_6$  has a higher Debye temperature than  $\text{Rb}_2\text{SeBr}_6$ . This clearly shows that  $\text{Rb}_2\text{SeCl}_6$  will have a strong temperature resistance due to its lattice vibration [1, 58, 59]. The increase in temperature can help in the thermodynamic stability of the studied double perovskite materials.

Table 2: Calculated values of elastic properties of  $\text{Rb}_2\text{SeX}_6$  ( $\text{X}=\text{Br}, \text{Cl}$ ) double perovskite using GGA-PBE and GGA-PBESol.

Mechanical Property	$\text{Rb}_2\text{SeBr}_6$	$\text{Rb}_2\text{SeBr}_6$	Other Works	$\text{Rb}_2\text{SeCl}_6$	$\text{Rb}_2\text{SeCl}_6$	Other Works
	PBE	PBESol		PBE	PBESol	
$C_{11}(\text{GPa})$	11.8	20.22	9.7 [9], 24.5 [18]	16.82	21.19	14.8 [9], 26 [18]
$C_{12}(\text{GPa})$	8.15	9.6	2.2 [9], 13 [18]	7.52	9.0	5.08 [9], 13.5 [18]
$C_{44}(\text{GPa})$	5.65	9.13	7.2 [9], 11.4 [18]	6.3	9.74	6.7 [9], 12.4 [18]
$C_{12} - C_{44}$	2.5	0.47	-	1.22	-0.74	-
$B$ (GPa)	9.37	13.14	5.0 [9], 16.8 [18]	10.62	23.06	8.8 [9], 17.6 [18]
$G_V$ (GPa)	3.60	7.60	-	5.62	7.88	-
$G_r$ (GPa)	3.08	7.09	-	5.52	7.59	-
$G$ (GPa)	3.6	7.34	4.9 [9], 8.6 [18]	5.62	7.73	6.4 [9], 9.4 [18]
$A$	3.09	1.71	1.98 [18]	1.35	1.59	-
$\xi$	0.391	0.60	-	0.345	0.55	-
$Y$	9.56	18.57	11.2 [9], 22.1 [18]	14.34	19.38	15.5 [9], 23.9 [18]
$\nu$	0.32	0.26	0.14 [9], 0.28 [18]	0.27	0.25	0.21 [9], 0.27 [18]
$R_P$	2.6	1.78	-	1.88	1.68	-
$R_f$	0.38	0.55	-	0.52	0.59	-
$\Theta_D$ (K)	97.091	136.9	-	150.2	172.5	-

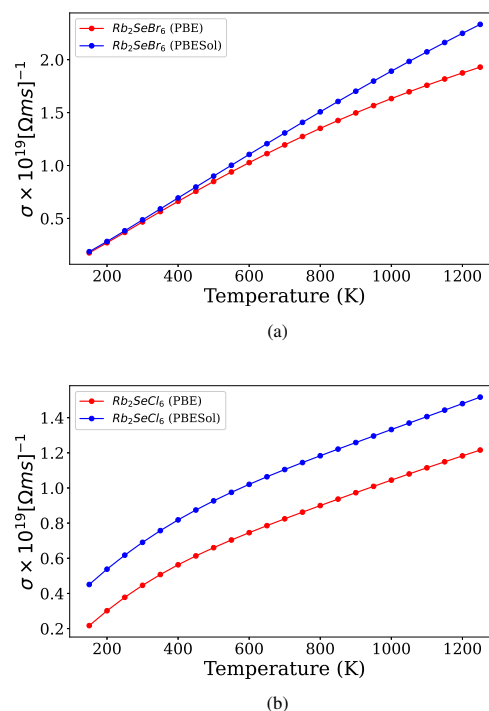
### 3.4. Thermo-electric Properties

Materials that have thermo-electric properties are being studied for use in converting thermal energy to electrical energy. The charge movement for energy transfer generates a heat gradient, which creates a potential difference and a thermo-electric effect [38]. Thermo-electric materials are widely used in a variety of practical applications, including thermo-electric refrigerators, detectors, and cooling systems [38, 60]. Perovskites materials are widely used for this purpose due to their low thermal conductivity and high electronic conductivity [38, 60, 61]. Materials with a narrow band gap semiconductor can also be used for thermo-electric applications [60, 62]. Semiconductors, in general, have a high Seebeck coefficient and low thermal conductivity, whereas antiperovskites, such as  $\text{Sr}_3\text{SbN}$ , are semiconductors with a bandgap of 1.15 eV and high thermopower and power factor [63, 64]. The bandgap of most high performance thermoelectric materials is around 0.5-1.5 eV [63, 64]. A material's band gap has a significant influence on the temperature-dependent electrical and thermal conductivities, Seebeck coefficient ( $S$ ), and other associated parameters. High band gap materials have higher  $S$  values, and vice versa.

#### 3.4.1. Electrical conductivity

The calculated electrical conductivity ( $\sigma$ ) for  $\text{Rb}_2\text{SeX}_6$  ( $\text{X}=\text{Cl}, \text{Br}$ ) are shown in Figure 15. In the figure, electrical conductivity ( $\sigma$ ) was plotted against temperature in the range of 150-1300 K. The Figure indicates that the electrical conductivity increases with increase in temperature; this is due to thermal excitation of electrons to the conduction band. High electrical conductivity materials are preferred for thermo-electric applications because they reverse the Joule heating effect [60]. Figure 15 indicates that  $\sigma$  increases

with increasing temperature; this trend holds true for the two exchange correlation functionals and the two double perovskite materials. According to the plots,  $\text{Rb}_2\text{SeBr}_6$  has a higher electrical conductivity value than  $\text{Rb}_2\text{SeCl}_6$ .

Figure 15: Electrical conductivity plots of (a)  $\text{Rb}_2\text{SeBr}_6$  and (b)  $\text{Rb}_2\text{SeCl}_6$  using GGA-PBE and GGA-PBESol.

### 3.4.2. Thermal conductivity

Thermal conductivity  $\kappa_e$  is another thermo-electric property parameter that combines the effect of electronic ( $\kappa_e$ ) and lattice thermal conductivity ( $\kappa_l$ ). Only the electronic contribution of thermal conductivity is calculated by the BoltzTrap2 code [37]. A good thermo-electric material has a low carrier resistance, which results from lower thermal conductivity, resulting in less carrier collision and heating [65]. Electronic thermal conductivity calculated for  $\text{Rb}_2\text{SeX}_6$  ( $X=\text{Br}, \text{Cl}$ ) using GGA-PBE and GGA-PBESol are shown in Figure 16. From the plots, the computed electronic thermal conductivity increases with temperature.  $\text{Rb}_2\text{SeBr}_6$  has higher electronic thermal conductivity values than  $\text{Rb}_2\text{SeCl}_6$  at high temperatures. Very good thermo-electric materials have ratio of thermal to electrical conductivity ( $\kappa_e/\sigma$ ) to be very small [1, 66, 67]. Thermal to electrical conductivity ratio of the two studied double perovskite materials is of the order of  $10^{-5}$ ; this suggests that both  $\text{Rb}_2\text{SeBr}_6$  and  $\text{Rb}_2\text{SeCl}_6$  are appropriate for thermo-electric applications.

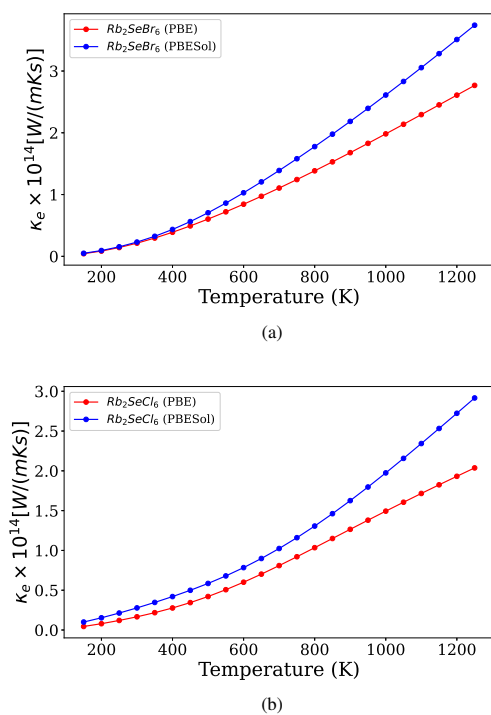


Figure 16: Thermal conductivity plots of (a)  $\text{Rb}_2\text{SeBr}_6$  and (b)  $\text{Rb}_2\text{SeCl}_6$  using GGA-PBE and GGA-PBESol.

### 3.4.3. Seebeck coefficients

Seebeck coefficient ( $S$ ), also known as thermopower, is another important parameter related to material electronic structure. It is defined as the magnitude of an induced thermo-electric voltage caused by a temperature gradient within the material [68]. Depending on the material, thermopower can be positive or negative. The dominant hole charge carrier is represented by positive Seebeck coefficients, while the dominant electron charge carrier is represented by negative Seebeck co-

efficients. The plots of calculated Seebeck coefficients of the studied double perovskite materials are shown in Figure 17. The Seebeck coefficient values for  $\text{Rb}_2\text{SeBr}_6$  and  $\text{Rb}_2\text{SeCl}_6$  are decreasing with increasing temperature, with minimum Seebeck coefficient values of  $0.198 \times 10^3$  (m V/K), and  $0.166 \times 10^3$  (m V/K) at 750 K, respectively.  $\text{Rb}_2\text{SeBr}_6$  has higher Seebeck coefficient values than  $\text{Rb}_2\text{SeCl}_6$  at high temperatures. All the calculated Seebeck coefficient values of the studied double perovskite are positive, indicating that the studied double perovskite compounds have p-type conduction.

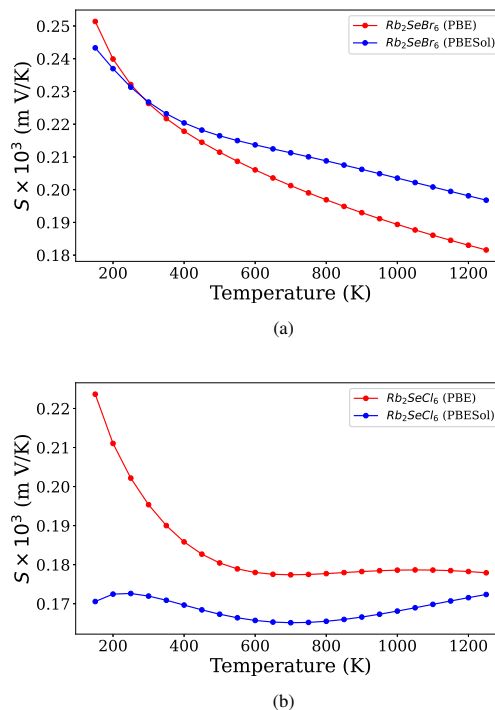


Figure 17: Seebeck coefficients plots of (a)  $\text{Rb}_2\text{SeBr}_6$  and (b)  $\text{Rb}_2\text{SeCl}_6$  using GGA-PBE and GGA-PBESol.

### 3.4.4. Power factor

Power factor defines the efficiency of a material for thermo-electric applications [39]. If a material has a high PF, it will extract heat effectively [69, 70]. The plot of power factor versus temperature range of 150 - 1300 K for  $\text{Rb}_2\text{SeX}_6$  ( $X=\text{Br}, \text{Cl}$ ) double perovskite materials using two different exchange correlation functionals are shown in Figure 18. For all exchange correlation functionals, the PF of the investigated double perovskite materials rises with temperature up to 1300 K;  $\text{Rb}_2\text{SeBr}_6$  has a PF value of  $9.10 \times 10^{14}$  W/m $^2$ s (PBESol) and  $6.20 \times 10^{14}$  W/m $^2$ s (PBE), but  $\text{Rb}_2\text{SeCl}_6$  has a PF value of  $4.60 \times 10^{14}$  W/m $^2$ s (PBESol) and  $3.80 \times 10^{14}$  W/m $^2$ s (PBE). PF studies clearly show that  $\text{Rb}_2\text{SeBr}_6$  double perovskite is more effective in thermoelectric conversion than the  $\text{Rb}_2\text{SeCl}_6$  double perovskites because it has higher PF values than  $\text{Rb}_2\text{SeCl}_6$ .

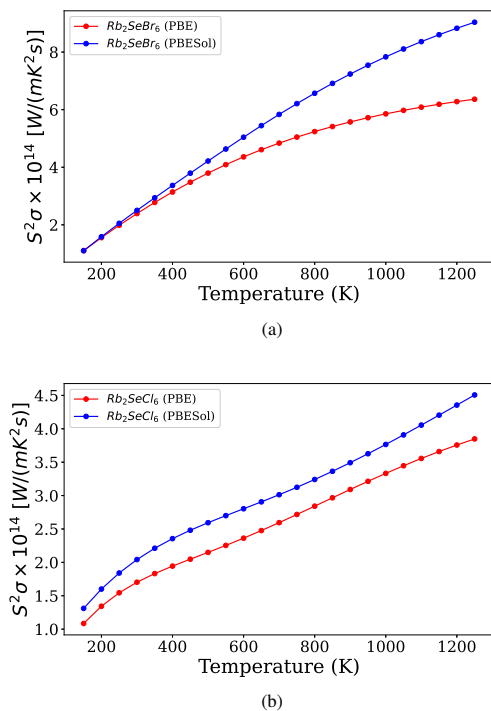


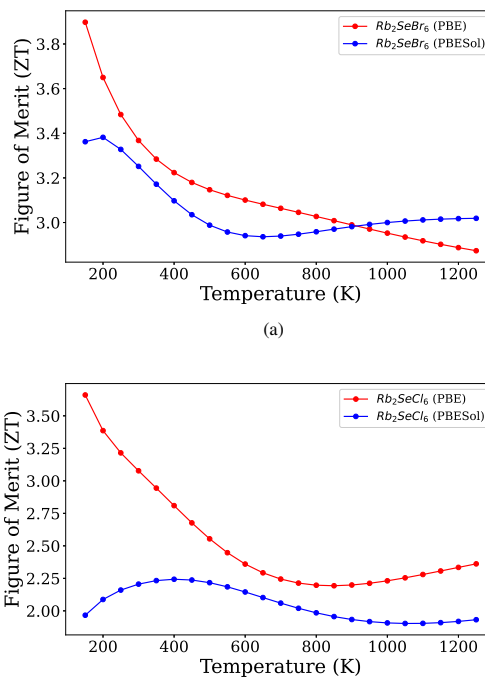
Figure 18: Power factor plots of (a)  $\text{Rb}_2\text{SeBr}_6$  and (b)  $\text{Rb}_2\text{SeCl}_6$  using GGA-PBE and GGA-PBESol

### 3.4.5. Figure of merit

The dimensionless figure of merit (ZT) is commonly used to calculate the efficiency of a thermo-electric material [71]. The figure of merit combines a number of material properties that must be optimized in order to create an efficient thermo-electric generator. A material with  $ZT \geq 1$  is a good thermo-electric material and suitable for device engineering [38, 72, 73]. The plots of calculated ZT against temperature in the range of 150 - 1300 K are shown in Figure 19. According to the plots, the calculated figure of merit values at all temperature range considered are greater than one for both  $\text{Rb}_2\text{SeBr}_6$  and  $\text{Rb}_2\text{SeCl}_6$ .  $\text{Rb}_2\text{SeBr}_6$  have higher ZT values than  $\text{Rb}_2\text{SeCl}_6$ . It can be concluded that the studied double perovskite materials are good thermo-electric material and suitable for device engineering. From all the results of TE properties,  $\text{Rb}_2\text{SeBr}_6$  exhibit better thermoelectric properties than  $\text{Rb}_2\text{SeCl}_6$ .

## 4. Conclusion

The parameterized GGA-PBE and GGA-PBESol exchange correlation functionals were used to examine the optoelectronic, elastic, and thermo-electric properties of  $\text{Rb}_2\text{SeX}_6$  ( $X=\text{Cl}, \text{Br}$ ) utilizing plane wave methods as implemented in the Quantum-Espresso code. The results of the electronic properties calculations revealed that both  $\text{Rb}_2\text{SeBr}_6$  and  $\text{Rb}_2\text{SeCl}_6$  double perovskite materials are indirect band gap semiconductors. The band gap values of  $\text{Rb}_2\text{SeBr}_6$  are relatively close to the two most studied organic perovskite



(b) Seebeck coefficients plots of (a)  $\text{Rb}_2\text{SeBr}_6$  and (b)  $\text{Rb}_2\text{SeCl}_6$  using GGA-PBE and GGA-PBESol.

Figure 19: Figure of merit plots of (a)  $\text{Rb}_2\text{SeBr}_6$  and (b)  $\text{Rb}_2\text{SeCl}_6$  using GGA-PBE and GGA-PBESol

( $\text{NH}_2\text{CH}=\text{NH}_2\text{PbI}_3$ )  $\text{FAPbI}_3$  and ( $\text{CH}_3\text{NH}_3\text{PbI}_3$ )  $\text{MAPbI}_3$ , and very close to the Shockley-Queisser theory of optimum band gap energy ( $E_g$ ) for high efficiency solar cells, which are in the range of 1.3 eV to 1.4 eV. The conductivity results show that the examined double perovskite materials have good values for electron generation. They have high absorption coefficients and a wider absorption range, making them potential materials for use in the optoelectronic industry. The calculated bulk moduli, shear moduli, Young moduli, and poisson's ratios for  $\text{Rb}_2\text{SeBr}_6$  and  $\text{Rb}_2\text{SeCl}_6$  indicate that they are ductile in nature. Due to high Debye temperature,  $\text{Rb}_2\text{SeCl}_6$  hypothetically has more resistance to temperature than  $\text{Rb}_2\text{SeBr}_6$ . Thermal to electrical conductivity ratio of the two materials is small (of the order of  $10^{-5}$ ), suggesting that the two double perovskite materials are appropriate for thermo-electric applications. The calculated Seebeck coefficient values are positive, meaning that they have p-type conduction. Figure of merit results indicate that  $\text{Rb}_2\text{SeX}_6$  ( $X=\text{Cl}, \text{Br}$ ) are good thermo-electric materials and  $\text{Rb}_2\text{SeBr}_6$  exhibit better thermoelectric properties than  $\text{Rb}_2\text{SeCl}_6$ .

## Acknowledgements

The authors would like to thank the Department of Physics and Materials Science at Kwara State University, Malete, for providing the computational resources utilized in some part of this study.

## References

- [1] A. B. Siad, M. Biara, & M. B. Siad, "Structural mechanical optoelectronic and thermoelectric properties of double perovskite compounds  $Cs_2TeX_6$  ( $X=Br, I$ ) for energy storage applications: First principles investigation", *Journal of Physics and chemistry of solids* **152** (2021) 109955.
- [2] Q. Mahmood, M. H. Alhossainy, M. S. Rashid, T. H. Flemban, H. Althib, T. Alshahrani, M. Rashid, & A. Laref, "First-principles study of lead-free double perovskites  $Rb_2TeX_6$  ( $X=Cl, Br, I$ ) for solar cells and renewable energy", *Materials Science and Engineering B* **266** (2021) 115064.
- [3] W. J. Yin, B. Weng, J. Ge, Q. Sun, Z. Li, & Y. A. Yan, "Oxide perovskites, double perovskites, and derivatives for electrocatalysis, photocatalysis, and photovoltaics", *Energy Environ. Sci.* **12** (2019) 442.
- [4] A. A. P. Mansur, H. S. Mansur, C. Tabare, A. Paiva, N. S. V. Capanema, "Eco-friendly  $AgInS_2/ZnS$  quantum dot nanohybrids with tunable luminescent properties modulated by pH-sensitive biopolymer for potential solar energy harvesting applications", *Journal of Materials Science: Materials in Electronics* **30** (2019) 16702, 10.1007/s10854-019-00719-0.
- [5] A. Yerudkar, M. Nair, H. D. Vishwanath, V. P. Sudhir, D. D. Vineeta, B. J. Jyeshtharaj, "Development of inexpensive, simple and environment-friendly solar selective absorber using copper nanoparticle", *International Journal of Chemical Reactor Engineering* **19** (2021) 727, doi:10.1515/ijcre-2020-0154.
- [6] K. C. Bhamu, A. Soni, & J. Sahariya, "Revealing optoelectronic and transport properties of potential perovskites  $Cs_2PdX_6$  ( $X=Cl, Br$ ): A probe from density functional theory (DFT)", *Solar Energy* **162** (2018) 336.
- [7] A. A. Sholagberu, W. A. Yahya, & A. A. Adewale, "Pressure effects on the opto-electronic and mechanical properties of the double perovskite  $Cs_2AgInCl_6$ ", *Phys. Scr.* **97** (2022) (085824).
- [8] A. A. Adewale, A. Chik, O. K. Yusuf, S. A. Ayinde, & Y. K. Sanusi, "First principle calculation of structural, electronic and optical properties of cds and doped  $Cd_{x-1}A_xS$  ( $A=Co, Fe, Ni$ ) compounds", *Materials Today Communications* **26** (2021) 101882.
- [9] X. Diao, Y. Diao, Y. Tang, G. Zhao, Q. X. Gu, Y. Shi, P. Zhu, & I. Zhang, "High-throughput screening of stable and efficient double inorganic halide perovskite materials by DFT", *Scientific Reports* **12** (2022) 12633.
- [10] F. I. H. Alias, M. H. Ridzwan, M. K. Yaakob, C. W. Loy, & Z. Mohamed, "Structural, electronic and optical studies of  $SrNiTeO$  double perovskite by first-principle DFT - LDA + U calculation", *Journal of Materials Research and Technology* **18** (2022) 1623.
- [11] R. Chaurasiya, S. Auluck, & A. Dixit, "Cation modified a (ba, sr and ca) znwo cubic double perovskites: A theoretical study", *Computational Condensed Matter* **14** (2018) 27.
- [12] M. K. Kim, J. Y. Moon, S. H. Oh, D. G. Oh, Y. J. Choi, & N. Lee, "Strong magnetoelectric coupling in mixed ferrimagnetic-multiferroic phases of a double perovskite", *Sci. Rep.* **9** (2019) 1.
- [13] L. Schade, S. Mahesh, G. Volonakis, M. Zacharias, B. Wenger, F. Schmidt, S. V. Kesava, D. Prabhakaran, M. Abdi-Jalebi, M. Lenz, F. Giustino, G. Longo, P. G. Radaelli, & H. J. Snaith, "Crystallographic, optical, and electronic properties of the  $Cs_2AgBi_{1-x}InxBi_6$  double perovskite: Understanding the fundamental photovoltaic efficiency challenges", *ACS Energy Lett.* **6** (2021) 1073.
- [14] Z. Xia, Y. Liu, & L. Manna, "Lead-free double perovskite  $Cs_2AgInCl_6$ ", *Ange wandte Chemie, WILEY-VCH*, (2020).
- [15] I. Deretzis, A. Alberti, G. Pellegrino, E. Mecca, F. Giannazzo, N. Sakai, T. Miyasaka, & A. La Magna, "Atomistic origins of  $CH_3NH_3PbI_3$  degradation to  $PbI_2$  in vacuum", *J. Appl. Phys. Lett.* **106** (2015) 131904.
- [16] L. Bertoluzzi, "Light induced structural changes in  $CH_3NH_3PbI_3$  perovskite solar cells", *J. Phys.: Conf. Ser.* **609** (2015) 012001.
- [17] G. Sadoughi, D. E. Starr, E. Handick, S. D. Stranks, M. Gorgoi, R. G. Wilks, M. Baer, & H. Snaith, "Observation and mediation of the presence of metallic lead in organic-inorganic perovskite films", *J. ACS Appl. Mater. Interfaces* **7** (2015) 13440.
- [18] W. Li, S. Zhu, Y. Zhao, & Q. Y. Yongqing, "Structural, electrical, optical properties and stability of  $Cs_2InBr_3-yXy \cdot H_2O$  ( $X=Cl, I, y=0.1, 2, 3, 4, 5$ ) perovskites: the first principles investigation. *Thin Solid Films* **733** (2021) 138805.
- [19] P. Giannozzi, S. Baroni, N. Bonini, M. Calandra, R. Car, C. Cavazzoni, D. Ceresoli, G. L. Chiarotti, M. Cococcioni, I. Dabo, A. Dal-Corso, S. de Gironcoli, S. Fabris, G. Fratesi, R. Gebauer, U. Gerstmann, C. Gougoussis, A. Kokalj, M. Lazzeri, L. Martin-Samos, N. Marzari, F. Mauri, R. Mazzarello, S. Paolini, A. Pasquarello, L. Paulatto, C. Sbraccia, S. Scandolo, G. Sclauzero, A. P. Seitsonen, A. Smogunov, P. Umari, & W. R. M., "Quantum espresso: a modular and open-source software project for quantum simulations of materials", *J. Phys.: Condens. Matter*, **21** (2009) 395502.
- [20] P. Giannozzi, M. Andreussi, T. Brumme, O. Bunau, M. Buongiorno Nardelli, M. Calandra, R. Car, C. Cavazzoni, D. Ceresoli, M. N. C. Cococcioni, I. Carnimeo, A. Dal-Corso, S. de Gironcoli, P. Delugas, J. R. A. DiStasio, A. Ferretti, A. Floris, G. Fratesi, G. Fugallo, R. Gebauer, U. Gerstmann, F. Giustino, T. Gorni, J. Jia, M. Kawamura, H. Y. Ko, F. A. Kokalj, E. Küçükbenli, M. Lazzeri, M. Marsili, N. Marzari, F. Mauri, N. L. Nguyen, H. V. Nguyen, A. Otero-de-la Roza, L. Paulatto, S. Ponce, D. Rocca, R. Sabatini, B. Santra, M. Schlip, A. P. Seitsonen, A. Smogunov, I. Timrov, T. Thonhauser, P. Umari, N. Vast, X. Wu, & S. Baroni, "Advanced capabilities for materials modelling with quantum espresso", *J. Phys.: Condens. Matter* **29** (2017) 465901.
- [21] J. P. Perdew, K. Burke, & M. Ernzerhof, "Generalized gradient approximation made simple", *Phys. Rev. Lett.* **77** (1996) 3865.
- [22] J. D. Pack, & H. J. Monkhorst, "Special points for brillouin-zone integrations"-a reply", *Phys. Rev. B Condens. Matter Mater. Phys.* **16** (1977) 1748.
- [23] C. G. Broyden, "The convergence of a class of double-rank minimization algorithms 1. general considerations", *IMA J. Appl. Math. (Institute Math. Its Appl.)* **6** (1970) 76.
- [24] C. G. Broyden, "The convergence of a class of double-rank minimization algorithms: 2. the new algorithm", *IMA J. Appl. Math. (Institute Math. Its Appl.)* **6** (1970) 222.
- [25] P. D. Mayengbam, R. S. Manas, K. Aparna, D. Prahlad, D. Madhumita, & P. Narendra, "Influence of microwave cooking on approximate, mineral and radical scavenging activities of tree bean seeds pods", *International Journal of current microbiology and applied sciences* **7** (2018) 3909.
- [26] M. Huma, M. Rashid, Q. Mahmood, E. Algrafy, N. A. Kattan, A. Laref, & A. S. Bhatti, "Physical properties of lead-free double perovskites  $A_2SnI_6$  ( $A=Cs, Rb$ ) using ab-initio calculations for solar cell applications", *Materials Science in Semiconductor Processing* **121** (2020) 1369.
- [27] S. Zhao, C. Lan, J. Ma, S. Pandey, S. Hayase, & T. Ma, "First principles study on the electronic and optical properties of B-site-ordered double perovskite  $Sr_2MMoO_6$  ( $M=Mg, Ca$  and  $Zn$ )", *Solid State Communications* **213-214** (2015) 19.
- [28] A. Abdulganiyu, "Elastic and optoelectronic study of the double perovskites  $Cs_2PdX_6$  ( $X=Br, Cl$ )", Master's thesis, Kwara State University, Malete, Nigeria, (2020).
- [29] S. Shah, Z. Ali, S. Mehmood, I. Khan, & I. Ahmad, "Electronic structure, optical and magnetic properties of double perovskites  $La_2MTiO_6$  ( $M=Co, Ni, Cu$  and  $Zn$ )", *Materials Chemistry and Physics* **272** (2021) 125050.
- [30] P. Blaha, K. Schwarz, G. K. H. Madsen, D. Kvasnicka, J. Luitz, R. Laskowski, F. Tran, & L. D. Marks, "An augmented plane wave plus local orbitals program for calculating crystal properties: Wien2k", *J. Phys.* **474** 23474 (2019).
- [31] S. A. Dar, V. Srivastava, U. Kumar, U. K. Sakalle, A. Vanshree, A., & V. Parey, "Electronic structure, magnetic, mechanical and thermophysical behavior of double perovskite  $Ba_2MgOsO_6$ ", *Eur. Phys. J. Plus* **133** (2018) 64.
- [32] M. Born, K. Huang, & M. Lax, "Electronic structure, magnetic", *Am. J. Phys* **23** (1955) 474.
- [33] M. K. Butt, M. Yaseen, I. A. Bhatti, J. B. M. Iqbal, A. Murtaza, M. Iqbal, M. M. AL-Anazy, M. H. Alhossainy, & A. L. "A DFT study of structural, magnetic, elastic and optoelectronic properties of lanthanide based  $XAlO_3$  ( $X=Nd, Gd$ ) compounds", *Journal of Materials Research and Technology*, **9** (2020) 16488.
- [34] A. Reuss, "Berechnung der fließgrenze von mischkristallen auf grund der plastizitätsbedingung für einkristalle", *ZAMM-Journal of Applied Mathematics and Mechanics/Zeitschrift für Angewandte Mathematik und Mechanik*, **9** (1929) 49.
- [35] R. Hill, "The elastic behaviour of a crystalline aggregate", *Proceedings of the Physical Society*, **65** (1952) 349.
- [36] D. H. Chung, & W. R. Buessem, "The voigt-reuss-hill (VRH) approximation and the elastic moduli of polycrystalline  $ZnO$ ,  $TiO_2$  (rutile), and  $\alpha-Al_2O_3$ ", *Journal of Applied Physics* **39** (1968) 2777,

- <https://doi.org/10.1063/1.1656672>.
- [37] G. K. Madsen, J. Carrete, & M. J. Verstraete, "BoltzTraP2: A program for interpolating band structures and calculating semi-classical transport coefficients", *Comput. Phys. Commun.* **231** (2018) 140.
- [38] A. H. Reshak, "Bismuth-containing semiconductors GaAs<sub>1-x</sub>Bi<sub>x</sub> for energy conversion: Thermoelectric properties", *Materials Science in Semiconductor Processing* **148** (2022) 106850.
- [39] V. Kumar, M. Kumar, & M. Singh, "Investigation of electronic, mechanical and thermoelectric properties of quaternary heusler compounds Zr-RhTiZ(Z=In,Al)", *Materials Today: Proceedings* **62** (2022) 3811.
- [40] M. Tariq, M. A. Ali, A. Laref, A. & G. Murtaza, "Anion replacement effect on the physical properties of metal halide double perovskites Cs<sub>2</sub>AgInX<sub>6</sub>(X=F,Cl,Br,I)", *Solid State Communications*, **314-315** (2020) 113929.
- [41] Q. Bao, O. Sandberg, D. Dagnelund, S. Sanden, S. Braun, H. Aarnio, X. W. Liu, & M. F. "Trap-assisted recombination via integer charge transfer states in organic bulk heterojunction photovoltaics", *Advanced Functional Materials* **24** (2014) 6309.
- [42] V. D. Mihailetchi, P. W. M. Blom, J. C. Hummelen, & M. T. Rispens, "Cathode dependence of the open-circuit voltage of polymer:fullerene bulk heterojunction solar cells", *Journal of applied physics* **94** (2003) 10.
- [43] W. Shockley, & H. J. Queisser, "Detailed balance limit of efficiency of pn-junction solar cells", *J. Appl. Phys.* **32** (1961) 510.
- [44] J. Guillemoles, T. Kirchartz, D. Cahen, & U. Rau, "Guide for the perplexed to the Shockley-Queisser model for solar cells", *Nature Photonics* **13** (2019) 501, <https://doi.org/10.1038/s41566-019-0479-2>.
- [45] B. Y. Yang, J. M. Zhang, A. Ali, Y. H. Huang, & X. Wei, "Computational investigation of structural, magnetic, electronic and optical properties of the cluster Mn-X<sub>6</sub>(X=P,S,Cl,Br,I) doped monolayer WSe<sub>2</sub>", *Thin Solid Films* **732** (2021) 138793.
- [46] N. Zarabina, & R. Rasuli, "Electronic and optical properties of halide double perovskites under strain: a density functional study *Energy Sources Part A: Recovery Utilization and Environmental Effects*", *Energy Sources, Part A: Recovery, Utilization, and Environmental Effects* **43** (2020) 2443, <https://doi.org/10.1080/15567036.2020.1867672>.
- [47] P. A. Cox, "The electronic structure and chemistry of solids", A Clarendon Press Publication, Wolfgang Tremel (1988).
- [48] T. M. J. Abdulkadhim, S. A. A. Alsaati, M. H. Shinen, "Theoretical Investigation of Diameter Effects and Edge Configuration on the Optical Properties of Graphdiyne Nanotubes in the Presence of Electric Field", *J. Nig. Soc. Phys. Sci.* **5** (2023) 1083.
- [49] M. H. Alia, J. M. Islam, A. Kumer, S. Hossain, U. Chakmaa, D. Howlader, T. Islam, & T. Hossain, "Investigation of structural, electronic and optical properties of Na<sub>2</sub>InAgCl<sub>6</sub>, K<sub>2</sub>InAgCl<sub>6</sub>, and Rb<sub>2</sub>InAgCl<sub>6</sub>, lead-free halide double perovskites regarding with Cs<sub>2</sub>InAgCl<sub>6</sub>, perovskites cell and a comparative study by dft functionals", *Materials Research* **24** (2021) e20210086.
- [50] S. C. Onuegbu, S. S. Oluyamo, O. I. Olusola, "Influence of Bath pH values on the Structural and Optical Properties of Electrodeposited MgO Thin Films for Optoelectronic applications", *J. Nig. Soc. Phys. Sci.* **5** (2023) 931.
- [51] A. A. Adewale, A. Chik, T. Adam, T. M. Joshua, & M. O. Durwoju, "Optoelectronic behavior of ZnS compound and its alloy: A first principle approach", *Materials Today Communications.* **27** (2021) 102077.
- [52] H. Umm, G. Murtaza, & H. R. Hafiz, "Optoelectronic and thermal properties of cubic SiMO<sub>3</sub>(M=Sn,Pb) oxides for device application: a first principle study", *Optical and Quantum Electronics* **52** (2020) 466.
- [53] M. A. Lahiji, & A. A. Ziabari, "First-principle calculation of the elastic, band structure, electronic states, and optical properties of Cu-doped ZnS nanolayers", *Physica B Condens. Matter* **501** (2016) 146.
- [54] A. A. Adewale, A. Chik, T. Adam, O. K. Yusuff, S. A. Ayinde, & Y. K. Sanusi, "First principles calculations of structural, electronic, mechanical and thermoelectric properties of cubic ATiO<sub>3</sub> (A= Be, Mg, Ca, Sr and Ba) perovskite oxide", *Computational Condensed Matter* **28** (2021) e00562.
- [55] A. A. Audu, W. A. Yahya, & A. A. Abdulkareem, "ab-initio studies of the structural, electronic and mechanical properties of Zn<sub>1-x</sub>Cr<sub>x</sub>Te", *Physics memoir, Journal of theoretical and applied physics* **3** (2021) 38.
- [56] T. Jinzhong, Z. Yuhong, H. Hua, & W. Bing, "The effect of alloying elements on the structural stability, mechanical properties, and debye temperature of Al<sub>3</sub>Li: A first-principles study", *Materials* **11** (2018) 1471.
- [57] W. Qing, J. Peng, & X. Wang, X. "First principles investigation of pressure dependent stability, phonon, debye temperature, physical, mechanical and thermodynamic properties of Rh<sub>3</sub>Al intermetallic compound", *Molecular Simulation* **44** (2018) 1554.
- [58] R. Singh, & G. Balasubramanian, "Impeding phonon transport through super lattices of organic-inorganic halide perovskites", *RSC Adv.* **7** (2017) 37015.
- [59] M. Marathe, A. Grünebohm, T. Nishimatsu, P. Entel, & C. Ederer, "First-principles-based calculation of the electrocaloric effect in BaTiO<sub>3</sub>: A comparison of direct and indirect methods", *Phys. Rev. B.* **93** (2016) 054110.
- [60] R. Ullah, A. H. Reshak, & M. A. Ali, "Pressure-dependent elastomechanical stability and thermoelectric properties of MYbF<sub>3</sub>(M=Rb,Cs) materials for renewable energy", *Int J Energy Res.* **45** (2021) 8711.
- [61] N. A. Noor, Q. Mahmood, M. Rashid, B. Ul-Haq, A. Laref, & S. A. Ahmad, "ab-initio study of thermodynamic stability, thermoelectric and optical properties of perovskites ATiO<sub>3</sub>(A=Pb,Sn)", *J. Solid State Chem.* **263** (2018) 115.
- [62] I. H. Kim, "Mg<sub>2</sub>Biv: Narrow bandgap thermoelectric semiconductors", *J. Korean Phys. Soc.* **72** (2018) 1095.
- [63] L. D. Zhao, S. H. Lo, Y. Zhang, H. Sun, G. Tan, C. Uher, C. Wolverton, V. P. Dravid, & M. G. Kanatzidis, "Ultralow thermal conductivity and high thermoelectric figure of merit in SnSe crystals", *Science Nature* **508** (2014) 373.
- [64] J. P. Heremans, V. Jovic, E. S. Toberer, A. Saramat, K. Kurosaki, A. Charoenphakdee, S. Yamanaka, & G. J. Snyder, "Enhancement of thermoelectric efficiency in PbTe by distortion of the electronic density of states", *Journal of Science* **80** (2008) 554.
- [65] M. Hassan, I. Arshad, Q. M. "Computational study of electronic, optical and thermoelectric properties of X<sub>3</sub>PbO(X=Ca,Sr,Ba) anti-perovskites", *Semicond Sci Technol.* **32** (2017) 115002.
- [66] T. Ghrib, A. Rached, I. A. Al-naum, A. Albalawi, H. Ashiq, B. Ul-Haq, & Mahmood, Q. "A new lead free double perovskites K<sub>2</sub>Ti(Cl/Br)<sub>6</sub>: a promising materials for optoelectronic and transport properties; probed by DFT", *Materials Chemistry and Physics.* **264** (2021) 264.
- [67] Q. Mahmood, M. Hassan, T. H. Flemban, B. Ul-Haq, S. AlFaify, N. A. Kattan, A. Laref, "Optoelectronic and thermoelectric properties of double perovskite Rb<sub>2</sub>PtX<sub>6</sub>(X=Cl,Br) for energy harvesting: first-principles investigations", *J. Phys. Chem. solids.* **148** (2021) 109665.
- [68] A. H. Reshak, "Thermoelectric properties for aa - and ab - stacking of a carbon nitride polymorph (C<sub>3</sub>N<sub>4</sub>)", *RSC Adv.* **4** (2014) 63137.
- [69] M. Saeed, I. Ul-Haq, A. S. Saleemi, S. Ur-Rehman, B. Ul-Haq, A. R. Chaudhry, I. Khan, "First-principles prediction of the ground-state crystal structure of double-perovskite halides Cs<sub>2</sub>AgCrX<sub>6</sub>(X=Cl,Br, andI)", *Journal of Physics and Chemistry of Solids* **160** (2022) 110302, <https://doi.org/10.1016/j.jpcs.2021.110302>.
- [70] O. Benguerine, Z. Nabi, A. Hachilif, B. Bouabdallah, B. Benichou, "Bright future in optoelectronics, photovoltaics and thermoelectric using the double perovskites oxides BaSrMgB'O<sub>6</sub>(B'=Te,W)", *Computational Condensed Matter* **30** (2022) e00649, <https://doi.org/10.1016/j.cocom.2022.e00649>.
- [71] G. Woolman, *Computational investigations of thermoelectric properties of lead telluride, magnesium silicide, and magnesium stannide under high pressure and anisotropic stress*, PhD thesis, The University of Edinburgh, (2021).
- [72] O. Rabin, L. Yu-Ming, D. M. S, "Anomalous high thermoelectric figure of merit in Bi<sub>1-x</sub>Sb<sub>x</sub> nanowires by carrier pocket alignment", *Appl. Phys. Lett.* **79** (2001) 81.
- [73] T. Takeuchi, "Conditions of electronic structure to obtain large dimensionless figure of merit for developing practical thermoelectric materials", *Materials Transactions* **50** (2009) 2359.